Dual oxic-anoxic co-culture enables direct study of host-anaerobe interactions at the airway epithelial interface.

Patrick J. Moore[1], Talia D. Wiggen[1], Leslie A. Kent[1], Sabrina J. Arif[1], Sarah K. Lucas[1], Joshua R. Fletcher[1], Alex R. Villareal[1], Adam Gilbertsen[1], Scott M. O'Grady[2], Ryan C. Hunter[1*]

[1]Department of Microbiology & Immunology, University of Minnesota, 689 23rd Avenue SE, Minneapolis, MN 55455
[2]Department of Animal Science, University of Minnesota, 1364 Eckles Avenue, Saint Paul, MN 55108

*To whom correspondence should be addressed:

Ryan C. Hunter
Department of Microbiology & Immunology
Microbiology Research Facility, 3-115
University of Minnesota
689 23rd Avenue SE
Minneapolis, MN 55455
Tel: (612) 625-1402
Email: rchunter@umn.edu
Twitter: @hunter_lab

SUMMARY

Strict and facultative anaerobic bacteria are widely associated with both acute and chronic airway disease. However, their potential role(s) in disease pathophysiology remain poorly understood due to inherent limitations of existing models and conflicting oxygen demands between anaerobes and host cells. To overcome these limitations, we optimized a dual oxic-anoxic culture (DOAC) platform that maintains an oxygen-limited microenvironment at the epithelial interface while host cells are oxygenated basolaterally. This approach enables host-bacterial co-culture for ~24h, and here we demonstrate its utility via two applications. First, we show that anaerobe challenge results in epithelial mucus degradation, inflammatory marker gene expression, and enhanced pathogen colonization. Second, we combine DOAC with single cell RNA sequencing (scRNAseq) to reveal a cell type-specific transcriptional response of the airway epithelium to anaerobe infection. Together, these data illustrate the versatility of DOAC while revealing new insights into anaerobe-host interactions and their mechanistic contributions to airway disease pathophysiology.

Keywords: mucin, anaerobes, *Pseudomonas aeruginosa, Fusobacterium nucleatum,* airway epithelium, single-cell RNA sequencing

41 **INTRODUCTION**

42 Decades of clinical laboratory culture have focused on a limited set of pathogens associated
43 with acute and chronic airway disease (e.g., *Pseudomonas aeruginosa, Staphylococcus aureus,*
44 *Mycobacterium tuberculosis*). More recently, culture-independent sequencing studies of airway
45 microbiota have identified more complex bacterial signatures, lending evidence to polymicrobial
46 disease etiologies. Notably, oral-associated facultative and obligate anaerobes – *Fusobacterium,*
47 *Prevotella, Veillonella, Streptococcus* spp. – which are present at low densities in the healthy
48 respiratory tract[1-4], are both prevalent and abundant in chronic obstructive pulmonary disease
49 (COPD), cystic fibrosis (CF), non-CF bronchiectasis, sinusitis, tuberculosis, ventilator-associated
50 pneumonia, and other respiratory complications[5-10]. In each instance, development of hypoxic
51 microenvironments at the airway epithelial interface provides a niche for anaerobe proliferation, often
52 reaching densities equal to or greater than those of canonical pathogens.

53 Mechanistic contributions of anaerobic bacteria to airway disease remain poorly understood
54 though several roles have been proposed. In healthy individuals, anaerobe abundance in
55 bronchoalveolar lavage fluid correlates with expression of proinflammatory cytokines, elevated Th17
56 lymphocytes, and a blunted TLR4 response, implicating a compromised first line of defense against
57 bacterial infection[1]. Indeed, epidemiologic and *in vitro* data suggest that anaerobes may facilitate
58 secondary colonization by canonical airway pathogens. In non-CF bronchiectasis, *Prevotella* and
59 *Veillonella* positively correlate with Th17 cytokines and non-tuberculosis mycobacterial infection[11].
60 Similarly, in HIV subjects, anaerobes suppress expression of interferon gamma and IL-17A via
61 production of short-chain fatty acids (SCFAs) and are thought to impair the host response to
62 consequent *M. tuberculosis* colonization[9]. In CF, anaerobe-derived SCFAs increase with age and
63 disease progression[12], mediate excessive production of IL-8 by bronchial epithelial cells (in turn
64 promoting neutrophil mobilization)[13] and potentiate the growth and virulence of canonical CF
65 pathogens *in vitro*[14-15]. Anaerobe-dominated bacterial communities in the CF airways are more
66 commonly associated with milder disease[16], but they also increase in abundance during acute
67 disease flares prior to antibiotic therapy[17], implicating anaerobes in pathogenesis.

68 Direct studies of anaerobe-host and anaerobe-host-pathogen interactions have been limited
69 by a dearth of compatible laboratory methods. Animal models can poorly reflect chronic infection
70 pathologies and/or be prohibitively expensive for high throughput analyses. As an alternative, three-
71 dimensional (3-D) cell culture approaches have greatly expanded our knowledge of microbial-
72 epithelial interactions[18-20]. However, incorporation of anaerobic microbiota into these models is
73 restricted by the inherent challenge of maintaining host cell viability under oxygen-limited culture
74 conditions. New *in vitro* approaches are needed for a more detailed understanding of anaerobic
75 microbiota and their interactions with airway epithelium.

76 Here we optimized a dual oxic-anoxic culture (DOAC) platform that recapitulates an oxygen
77 limited epithelial microenvironment thought to exist in the diseased airways[21-22]. In this platform,
78 polarized epithelial monolayers are maintained at air-liquid interface in an anaerobic chamber while
79 O_2 and CO_2 are delivered to the culture apparatus from an external source. This setup allows for
80 maintenance of hypoxia in the apical compartment while host cells are oxygenated basolaterally. We
81 establish the utility of this model through two *in vitro* studies of anaerobe-airway interactions. First,
82 we use the DOAC platform to test the hypothesis that anaerobic microbiota enhance colonization of
83 the epithelial surface by the canonical airway pathogen, *P. aeruginosa.* Second, we combine DOAC
84 with single-cell RNA sequencing (scRNAseq) to assess the cell type-specific transcriptional
85 response of normal human tracheal bronchial epithelial (nHTBE) cells to infection by *Fusobacterium*
86 *nucleatum* – an oral commensal with pathogenic potential[23]. Through this work we not only
87 demonstrate the power and versatility of the DOAC platform, but also offer new insight into
88 mechanisms of pathogen colonization and potential roles of anaerobic bacteria in the onset and
89 development of airway disease.

90

91 **RESULTS**

92 **Optimization of a dual oxic-anoxic epithelial culture (DOAC) platform**

93 Our primary objective was to establish and optimize a cell culture platform that facilitates
94 study of anaerobe-host interactions (**Fig. 1A, Fig. S1**). To do so, we first cultured polarized
95 monolayers of the adenocarcinoma cell line, Calu-3, at air-liquid interface (ALI) for 21-28 days under

96 standard (normoxic) conditions. As shown previously[24], polarized Calu-3s produce a distinct mucus
97 layer on the apical surface (**Fig. S1A**), mimicking aberrant mucin accumulation associated with CF,
98 COPD, sinusitis and other chronic airway diseases. Once polarized, cell cultures were placed in a
99 gas-permeable multi-well plate manifold (**Fig. S1B-D, Fig. S2**), transferred to an anaerobic chamber,
100 and mixed gas (21% O_2/ 5% CO_2/ 74% N_2) was delivered through a chamber cable gland to the
101 basolateral compartment of the Transwell-containing plate. This dual oxic-anoxic culture (DOAC)
102 format achieves oxygenation of host cells while maintaining exposure of the apical surface to the
103 oxygen-limited environment of the anaerobic chamber. Using DOAC we determined that, when
104 compared to cell culture under normoxic and strict anoxic conditions, cytotoxicity was negligible up
105 to 24h as determined by lactate dehydrogenase (LDH) release, with a progressive increase in cell
106 death after 48h and 72h (**Fig. 1B)**. Viability of the immortalized RPMI 2650 nasal cell line and primary
107 human tracheal bronchial epithelial cells (nHTBE) was similarly achieved under DOAC conditions for
108 at least 24h (**Fig. 1C).**

109 We then determined the effects of DOAC, if any, on Calu-3 cell physiology after 24h, which
110 was chosen as our time point for downstream experiments. Transepithelial electrical resistance
111 (TEER) (**Fig. 1D**) and E-cadherin concentrations (**Fig. 1E**), both proxies of epithelial barrier integrity,
112 showed slight but insignificant decreases under DOAC conditions (P=0.21 and 0.70, respectively).
113 These data were corroborated by immunofluorescence microscopy which revealed confluent
114 monolayers and well-defined staining of tight junction zonula occludens proteins that appeared as
115 near-continuous rings at the periphery of each cell (**Fig. 1F**). Previous work has shown hypoxia-
116 induced expression of pro-inflammatory cytokines in pulmonary fibroblasts[25]. Thus, we also used an
117 enzyme-linked immunosorbent assay to quantify IL-6 and IL-8 production by Calu-3 cells. Both
118 cytokines showed no significant increases under DOAC conditions relative to controls (**Fig. 1G, H**,
119 P=0.54 and 0.68, respectively), suggesting that our culture conditions do not elicit an inflammatory
120 response after 24h.

121 To gain a broader understanding of the physiological response of Calu-3 cells to dual oxic-
122 anoxic culture, we used bulk RNAseq to compare global Calu-3 gene expression to culture under
123 normoxic conditions. Transcriptome analysis revealed 148 differentially expressed transcripts (117

124 upregulated, 31 downregulated, l2fc ≥ 1, adjusted *P*<0.001; out of ~16,000 total genes) (**Fig. 2A,**
125 **Data S1**). With the exception of *ANGPTL4* (encoding angiopoietin-like 4) and *SERPINA1* (alpha-1
126 antitrypsin) (**Fig. 2B**), which are induced in response to hypoxia and acute inflammation,
127 respectively, few markers of cell stress were differentially expressed, including genes involved in
128 tight junction formation, oxidative stress, and endoplasmic reticulum stress. Importantly, HIF-1α,
129 which is constitutively expressed at low levels under normoxia but upregulated under hypoxia, was
130 also consistent between culture conditions after 24h, suggesting that Calu-3 cells are sufficiently
131 oxygenated under DOAC conditions (**Fig. 2B**). Among inflammatory biomarkers, only *ICAM1*
132 (intracellular adhesion molecule 1) and *TGFβ1* (transforming growth factor beta 1) showed
133 statistically significant differences, further demonstrating that DOAC did not yield an appreciably
134 inflammatory microenvironment (**Fig. 2C**). Finally, since we would eventually use the DOAC model
135 to assay bacterial colonization of the apical mucus layer, we compared mucin-related gene
136 expression between conditions. Among detectable transcripts (*MUC1, MUC3A, MUC5AC, MUC5B,*
137 and *MUC13*), no significant differences were observed between culture conditions (**Fig. 2D**). These
138 data demonstrate that DOAC yields minor changes in cytotoxicity and gene expression after 24h,
139 but we consider these changes to be negligible relative to the value of the DOAC platform for
140 modeling anaerobe-epithelial interactions.
141
142 **Anaerobic airway microbiota promote an inflammatory host response**
143 The lack of tractable epithelial cell culture systems compatible with hypoxic or anoxic bacterial
144 growth has limited our understanding of host-anaerobe interactions. Prior work has shown that
145 culture supernatants of anaerobic bacteria elicit pro-inflammatory cytokine expression *in vitro*
146 through mixed-acid fermentation and production of SCFAs [1,12,13]. However, it is not yet known how
147 the host responds to the direct presence of anaerobes at the epithelial interface. To address this
148 knowledge gap, we used the DOAC platform to assess the response of Calu-3 cells to co-culture
149 with anaerobic microbiota.
150 As a starting point, we used a defined anaerobic bacterial consortium (ABC) derived from
151 airway mucus collected from an individual with chronic sinusitis. This representative community was

152 enriched under strict anaerobic culture conditions[15] and was chosen for its dominant bacterial taxa
153 (*Veillonella, Prevotella, Streptococcus*) associated with both healthy and diseased airways (**Fig. 3A**).
154 These genera are also known for their mucin-degradation capacity and the ability to support
155 pathogen growth through nutrient cross-feeding[14,15]. After 3h of equilibration under DOAC, Calu-3
156 cells were apically challenged with the anaerobically enriched bacterial consortium (~8 x 10^6 colony
157 forming units (CFUs)) and incubated for an additional 24h. Colonization of the apical interface was
158 confirmed and visualized using scanning electron microscopy (**Fig. 3B)**. Bacteria (3.6 x 10^6 CFUs)
159 were recovered after 24h by washing with PBS and plating on Brain Heart Infusion agar (BHI)(**Fig.
160 3C**), while washing with Triton X-100 resulted in a 0.8-log increase in recovery (2.4 x 10^7 CFUs),
161 suggesting both anaerobe growth at the epithelial surface and either robust attachment, disruption
162 of bacterial aggregates, or bacterial invasion of host cells (i.e., cells were not removed by gentle PBS
163 washing alone). Importantly, recovery of 8.1 x 10^5 CFUs on *Prevotella* selective media under anoxic
164 conditions (compared to 2.6 x 10^5 in the inoculum) confirmed that apical oxygen concentrations were
165 sufficiently low for strict anaerobe viability. We note that in contrast to the canonical airway pathogens
166 *S. aureus* and *P. aeruginosa* [26,27], Calu-3 cytotoxicity was not induced by anaerobe treatment after
167 24h (**Fig. 3D**).

168 We then used RNAseq to profile the Calu-3 transcriptional response to anaerobe challenge
169 (**Fig. 3E**, **Data S2**) which revealed the differential expression of various inflammatory biomarkers.
170 These included *ICAM1* (intercellular adhesion molecule 1, previously shown to be expressed in
171 response to periodontopathic bacteria)[28], *TNFAIP2* (mediated by TNFα in response to bacterial
172 challenge)[29], chemokines *CXCL1* and *CXCL5* (neutrophil chemoattractants primarily expressed as
173 an acute inflammatory response to infection)[30,31], and *SOD2* (superoxide dismutase 2, which is
174 expressed in response to lipopolysaccharide and has an antiapoptotic role against inflammatory
175 cytokines)[32]. Other inflammatory markers including *PI3* (elafin, an elastase inhibitor that can prime
176 innate immune responses in the lung)[33], *CXCL3* (neutrophil chemoattractant), *C3* (complement),
177 *CYP24A1* (cytochrome p450 family 24 subfamily A member 1), *OAS1* (oligoadenylate synthetase),
178 and *SDC4* (syndecan 4) were also differentially expressed, though did not reach our threshold
179 adjusted *P* value of <0.001 (**Fig. 3F**). These data demonstrate that while not cytotoxic, anaerobes

180 and/or their metabolic byproducts were detectable by host cells and elicit an inflammatory response.

181 **Anaerobic microbiota alter the mucosal interface via mucin degradation**

182 Our previous work demonstrated the ability of anaerobic microbiota to degrade airway mucins
183 and support the growth of canonical pathogens via nutrient cross-feeding[14,15]. Thus, in support of
184 downstream pathogen colonization experiments, we used fast protein liquid chromatography (FPLC)
185 to determine whether anaerobe challenge altered Calu-3 mucin integrity relative to unchallenged
186 cells. To do so, we collected and purified mucin from the apical side of the Transwells as previously
187 described[24] and used size-exclusion chromatography to assay their integrity. As expected,
188 chromatograms revealed two characteristic peaks; (i) high molecular weight mucins which ran in the
189 void volume of the column, and (ii) a broader inclusion volume peak representative of lower
190 molecular weight mucins[34] (**Fig. 4A**). While differences in the chromatographic profile of peak 1 (high
191 molecular weight mucins) were negligible between culture conditions (P=0.38), peak 2 area was
192 significantly reduced (P=0.043) following anaerobe challenge (**Fig. 4B**), reflecting proteolytic and/or
193 glycolytic degradation of lower-molecular weight mucin glycoproteins. These data suggest that in
194 addition to eliciting a pro-inflammatory host response, anaerobic colonization can alter the
195 physicochemical nature of the mucosal interface.

196

197 **Anaerobes promote *P. aeruginosa* colonization of the airway epithelium**

198 Viral challenge of the airway epithelium potentiates colonization by *P. aeruginosa* via
199 interferon mediated effects[18]. Other work has shown that the protective role of the mucus barrier is
200 compromised by *Streptococcus mitis* through hydrolysis of mucin glycans[35]. Given that the
201 anaerobically enriched consortium used in our model both elicits inflammation (**Fig. 3**) and alters
202 mucin integrity (**Fig. 4**), we hypothesized that in addition to providing nutrients for pathogen growth
203 through cross-feeding, anaerobes enhance *P. aeruginosa* colonization of the airway epithelium (**Fig.**
204 **5A**).

205 To test this hypothesis, Calu-3 cells were first treated with the anaerobic consortium (see **Fig.**
206 **3A**) for 24h, washed with PBS to remove spent medium and unbound cells, and subsequently
207 infected with ~5 x 10^7 CFUs of *P. aeruginosa* PA14 for 2h. Removal of spent medium and a short

208 incubation time ensured that any difference in colonization between anaerobe-treated cells and an
209 unconditioned (i.e., no anaerobe) control was a result of cell attachment and not enhanced growth
210 over time. *P. aeruginosa* colonization was then determined by washing and permeabilization of Calu-
211 3 cells followed by plate enumeration. As predicted, anaerobe pre-treatment resulted in an ~67.5%
212 increase in *P. aeruginosa* attachment (1.1 x 10^7 CFUs) relative to untreated controls (P=0.028, **Fig.**
213 **5B**), supporting our hypothesis that anaerobic microbiota can enhance pathogen colonization of the
214 airway mucosal interface.

215 To assess the contributions of individual anaerobes to *P. aeruginosa* colonization we then
216 challenged Calu-3 cells with representative isolates of the three most abundant genera in the
217 anaerobic consortium (*Streptococcus, Veillonella, Prevotella)* prior to *P. aeruginosa* colonization
218 (**Fig. 5D**). We found that *Streptococcus* species (*S. gordonii* and *S. parasanguinis*) had little effect
219 on PA14 colonization, despite their known mucolytic capacity. Similarly, *V. parvula,* an asaccharolytic
220 bacterium, resulted in no significant differences between treatment conditions. By contrast, challenge
221 with both *P. melaninogenica* and *P. oris,* two species commonly associated with inflammatory airway
222 disease[1,6,36], resulted in significantly increased PA14 recovery from Calu-3 cells compared to
223 unconditioned controls (P=0.004 and P=0.023, respectively). These data suggest that while
224 anaerobic microbiota of the respiratory tract facilitate enhanced colonization of the epithelium by *P.*
225 *aeruginosa*, they do so in a species-specific manner.

226

227 **Single cell RNA sequencing reveals cell-specific expression of inflammatory marker genes**
228 **and cancer-related pathways in response to *F. nucleatum***

229 A drawback to transcriptomic studies of epithelial cell populations (**e.g., Fig. 2A, Fig. 3E**) is
230 that bulk RNA sequencing averages out contributions of different cell types to the overall
231 transcriptional landscape. Not only does this mask how physiological processes are distributed
232 among cells, but contributions from rare cell types are also largely invisible. To address these
233 limitations, single-cell RNA sequencing (scRNAseq) has been widely adopted in respiratory research
234 and has already led to the discovery of ionocytes, the immune landscape of lung cancer, novel
235 mononuclear phagocytes in the CF lung, and the host response to SARS-CoV-2 infection[37-40]. To

236 our knowledge, scRNAseq has not yet been applied to bacterial-host interactions in the context of
237 airway disease. Given the many examples of tissue and cell-specific tropism exhibited by pathogens
238 of the respiratory tract[41-43], here we combined the DOAC platform with scRNAseq to test our
239 hypothesis that anaerobic microbiota elicit an inflammatory host response that varies by epithelial
240 cell type.

241 To test our hypothesis, primary human bronchial epithelial (nHTBE) cells were cultured
242 under normoxia, transferred to DOAC conditions for 3h, followed by apical challenge with
243 *Fusobacterium nucleatum* - both an anaerobic oral commensal and pathogen associated with a
244 spectrum of respiratory tract infections[23]. After 24h of co-culture, we captured nHTBEs using the 10X
245 Genomics Chromium controller **(Fig. 6A)** and sequenced an average of 2,007 cells per untreated
246 replicate (n=6) and 3,682 from each *F. nucleatum*-treated replicate (n=3). After removing cells with
247 less than 250 detectable genes and additional filtering criteria, we analyzed a total of 6,981 untreated
248 and 5,010 treated cells, with an average of 4,042 and 3,103 expressed genes per cell, respectively.
249 To identify main cell types, we performed a combined analysis of all cells from all samples using
250 uniform manifold approximation and partitioning (UMAP)[44,45]. This analysis partitioned cells into 13
251 distinct clusters based on gene expression profiles, colored accordingly in **Fig. 6B,** which did not
252 appreciably differ between treatments (**Fig. 6C; Fig. S3**). Clusters were manually identified post-hoc
253 by identifying genes significantly upregulated within each cluster and by comparison to established
254 sets of marker genes for canonical epithelial cell types (**Fig. 6D**)[37]. Among these clusters, we found
255 cell type-specific expression of 17 pattern recognition receptors (PRRs) that play a critical role in the
256 innate host response to microbial encounter (**Fig.6E; Fig.S3**). For example, toll-like receptor 2
257 (TLR2) was predominately expressed by secretory cells, while NOD1 and NLRP1 exhibited higher
258 expression in ciliated and basal cells, respectively. These data are consistent with previous reports
259 describing heterogeneous expression of PRRs across airway epithelial cell types[46,47] and supported
260 our hypothesis that the host response to bacterial challenge would also be cell type specific.

261 Using DESeq2[48], we then performed differential gene expression analysis, accounting for
262 both the effects of cell type and bacterial challenge. As predicted, comparison of *F. nucleatum*-
263 treated cells to untreated controls revealed a distinct, cell type-specific response to bacterial

264 challenge: basal, 34 up / 21 down; ciliated, 217 up / 23 down; and secretory cells, 77 up / 10 down
265 (padj > 0.001) (**Fig. 6F, Data S3**). Among notable differentially expressed genes, *F. nucleatum*
266 stimulated expression of multiple cytokines and chemokines, including tumor necrosis factor
267 superfamily member 15 (*TNFSF15*) in secretory cells, *CCL15* in ciliated cells, and inflammatory
268 marker genes encoding interferon regulatory factor (*IRF1*), matrix metalloproteases (*MMP1, MMP9*),
269 and *CXCL17* in basal cells (**Fig.6G**). These data are consistent with previous reports of Fusobacteria
270 stimulating inflammatory host responses in the oral cavity and diverse extra-oral body sites[49-52].
271 Unexpectedly, *F. nucleatum* challenge also resulted in a striking differential expression of cancer-
272 associated genes and pathways (**Fig.6H)**. *CYP1B1*, a universal cancer marker encoding cytochrome
273 P450 1B1[53], and *GSTA1* (glutathione S-transferase A1) which promotes lung cancer cell invasion
274 and adhesion[54], both increased in expression in each of basal, ciliated, and secretory cells in
275 response to *F. nucleatum* (**Fig. 6H)**. *HSPA1A* (encoding heat shock protein A), involved in the
276 promotion of tumor cell proliferation, metastasis, and invasion[55], was also upregulated in both basal
277 and ciliated cells. Twenty-one other cancer-related genes varied by cell type (padj < 0.001). While
278 *F. nucleatum* has been associated with late-stage lung cancer[56,57] and poor patient response to
279 immunotherapy[58], these data support a direct role for the bacterium in airway carcinogenesis. To our
280 knowledge, these data are the first to reveal the epithelial response to bacterial challenge with the
281 granularity afforded by scRNAseq and further demonstrate the power and versatility of the DOAC
282 platform to model anaerobe-host interactions.
283

284 **DISCUSSION**

285 The surge in culture-independent sequencing of human microbiota has spawned renewed
286 interest in the importance of anaerobic bacteria in disease etiologies. However, despite anaerobes
287 comprising a significant component of airway bacterial communities, studies on their contributions to
288 disease pathophysiology have reported seemingly contradictory results, calling into question their
289 role(s) in patient morbidity. Proposed pathogenic mechanisms are supported by compelling *in vitro*
290 data[12-14], but their relevance is unresolved due to a lack of compatible models with which to test their
291 interactions with the respiratory epithelium. To address this knowledge gap, here we optimized and

292 characterized a model platform (DOAC) that enables co-culture of strict and facultative anaerobes
293 with polarized airway epithelial cells. Importantly, provision of oxygen exclusively to the basolateral
294 side of host cells prevented anoxia-associated cytotoxicity, inflammation, and significant changes in
295 global gene expression, validating its utility for the study of anaerobe-host interactions. Using this
296 platform, we demonstrate that (i) anaerobic microbiota promote enhanced epithelial colonization by
297 *P. aeruginosa*, and (ii) that *F. nucleatum* elicits a pro-inflammatory and cancer-associated
298 transcriptional response that varies by epithelial cell type.

299 Disparate oxygen demands between epithelial cells and anaerobic bacteria pose significant
300 challenges for their co-culture *in vitro*. Several culture systems have been developed to overcome
301 these challenges and recapitulate an oxygen-restricted mucosal interface[59-61], though each has
302 limitations. Transwell cultures of Caco-2, HaCaT, and primary human gingival cells have been used
303 to demonstrate that anaerobic taxa can adhere to, invade, and alter oral and intestinal epithelia, yet
304 these assays are either limited to short incubation times or poorly mimic *in vivo* conditions[62-64]. Newer
305 microfluidic-based and 'organ-on-a-chip' models have also seen widespread interest due to their
306 ability to establish a dual oxic-anoxic interface and facilitate study of anaerobe-host interactions[65-68].
307 However, these models either preclude direct host-bacterial contact or are technically challenging to
308 maintain both oxic and strict anoxic microcompartments. The approach described here offers the
309 distinct advantages of ease-of-use, direct interactions between host and microbiota, reproducibility
310 given the multi-well plate format, and methodological flexibility lending itself to biochemical,
311 microscopy, and transcriptomic studies.

312 To demonstrate the utility of the DOAC platform, we first used an anaerobic polymicrobial
313 consortium representative of chronic airway disease. Dominated by *Streptococcus, Prevotella,* and
314 *Veillonella* spp.*,* this consortium (among other bacterial taxa) is thought to seed the airways through
315 microaspiration from the oral cavity and is recognized as a key risk factor in the development of
316 infection in COPD, CF, pneumonia, sinusitis and other diseases. For example, *in vitro* studies have
317 shown that anaerobe-derived supernatants containing proteases and pro-inflammatory short-chain
318 fatty acids modulate the immune tone of bronchial epithelial cell lines and primary cell cultures[12,13].
319 Indeed, anaerobe abundance in both diseased airways and healthy controls is associated with

320 enhanced expression of inflammatory cytokines[1,9]. Our data also support an immunomodulatory role
321 and suggest that anaerobe colonization of the airway mucosa may establish a local inflammatory
322 environment known to promote colonization by *P. aeruginosa* and other canonical pathogens[18,20].

323 We previously reported that anaerobes can also stimulate pathogen growth through mucin-
324 based cross-feeding[14,15]. Specifically, *P. aeruginosa* and *S. aureus,* which cannot efficiently
325 catabolize mucins in isolation, can gain access to bioavailable substrates via anaerobe-mediated
326 degradation of the mucin polypeptide and O-linked glycans. Though not directly tested here, it is
327 plausible that pre-colonization with an anaerobic bacterial community liberates additional mucin-
328 derived metabolites on which pathogens can thrive at the epithelial interface. While it remains unclear
329 why only low molecular weight mucins were altered (see Fig. 4), our FPLC data confirm that the
330 mucosal surface is structurally modified because of anaerobic colonization. Given that mucin
331 degradation has been shown to compromise its barrier function and enhance pathogen-epithelial
332 interactions[35], we propose that in addition to the host's impaired mucociliary clearance, pathogenic
333 contributions of anaerobic microbiota to airway infection are likely imparted through a multifactorial
334 process (e.g., inflammation, cross-feeding, and surface alteration).

335 By focusing on an early time point after *P. aeruginosa* challenge (2h), we targeted anaerobic
336 mucin degradation and its role in re-shaping the epithelial interface while enhancing pathogen
337 attachment, as was previously shown for *S. mitis* and *Neisseria meningitidis*[35]. As predicted,
338 anaerobe colonization resulted in a significant increase in *P. aeruginosa* attachment, likely mediated,
339 at least in part, by mucin degradation. This observation has important clinical implications. Most
340 notably, epithelial colonization is known to stimulate rapid *P. aeruginosa* biofilm maturation and
341 associated increases in extracellular polysaccharide production, induction of quorum-sensing and
342 other transcriptional changes[19]. In addition, *P. aeruginosa* grown on bronchial epithelial cells is far
343 more resistant to antibiotic treatment than when grown on abiotic surfaces[19], consistent with their
344 increased tolerance *in vivo*. We propose that anaerobe-mediated colonization further potentiates
345 these phenotypes. Moving forward, it will be important to consider *P. aeruginosa* interactions with
346 the host over longer time periods to further understand differences in pathogen physiology and the
347 inflammatory host response in the presence and absence of anaerobic microbiota.

348 We elected to test Calu-3 cells as a representative cell line for several reasons. First, Calu-3
349 cells reach polarization at ALI within ~21 days and achieve TEER values far greater and more stable
350 than those of primary cells (>1000 Ωcm^2) [69,70]. In addition, overproduction of mucus on the apical
351 surface of Calu-3 cells mimics a diseased mucosal environment and allowed us to test the hypothesis
352 that mucin degradation enhances pathogen colonization. This was an important consideration as *P.*
353 *aeruginosa* biofilms, at least in the context of CF, are thought to form within secreted mucus as
354 opposed to the epithelial layer [71]. We also acknowledge the limitations of using Calu-3 cells. Unlike
355 primary cells, which form a pseudostratified epithelium with mucociliary differentiation, Calu-3 cells
356 are derived from human bronchial submucosal glands that comprise a relatively homogenous
357 monolayer. Transcriptional and physiological responses to external stimuli may also be unique to
358 Calu-3s. As an example, *S. aureus* enterotoxin B is known to elicit significant differences in barrier
359 integrity as well as IL-6 and IL-8 production in Calu-3 cells relative to primary tissue[72]. These, among
360 other considerations, underscore the importance of using the DOAC platform with additional cell
361 lines and primary tissues to model anaerobe-host interactions in greater detail.

362 Indeed, the combined use of DOAC, primary bronchial epithelial cells, and scRNAseq
363 revealed the cell-type specific transcriptional response to *F. nucleatum* challenge. Generally
364 regarded as an abundant commensal of the oral cavity, there is growing recognition of *F. nucleatum*
365 as an emerging pathogen associated with airway infection[15], periodontal disease[73], adverse
366 pregnancy outcomes[74], and GI disorders[75]. In the latter instance, colonic biopsies from patients with
367 inflammatory bowel disease (IBD) carry a greater *F. nucleatum* burden, while strains isolated from
368 inflamed IBD tissues tend to be more invasive than those from healthy controls[76,77]. Accumulating
369 evidence also suggests its role in the progression of various cancers[78], including those of the breast,
370 oral cavity, esophagus, rectum, and colon, and data presented here likewise suggest a pro-
371 inflammatory and tumorigenic effect of *F. nucleatum* on the airway epithelium. Recent work
372 demonstrated that *Fusobacterium spp.,* among other oral microbiota, correlate with lower airway
373 inflammation and are enriched in advanced lung cancers[56,57]. However, to our knowledge, a direct
374 effect of *F. nucleatum* on cancer-associated pathways in the airways was previously unknown, as
375 was the cell type specific transcriptional response of the host. Whether *F. nucleatum* has a

376 colonization preference for specific cells over others requires further study, but the unique distribution
377 of PRRs between basal, secretory, and ciliated cells insinuates that detection of the bacterium and/or
378 its secreted metabolites, is at least partially responsible for the heterogeneous host response. If
379 immunomodulatory therapies are to be further developed and used clinically, understanding which
380 bacterial species promote or mitigate inflammation / tumorigenesis and how individual cells respond
381 will be critical information to have in-hand. The DOAC platform paves the way for further study of
382 these and other aspects of the host-anaerobe dynamic.

383 In summary, DOAC represents a tractable co-culture system that facilitates extended
384 interrogation of host-anaerobe interactions. While we use this model here to demonstrate a role for
385 anaerobic microbiota in pathogen colonization of the airways and how the airway epithelium
386 responds to oral-associated anaerobes, this work will undoubtedly benefit future studies focused on
387 anaerobe-host and anaerobe-host-pathogen interactions. Not only do we anticipate generating a
388 deeper understanding of our microbiota at the epithelial interface under oxygen-limited conditions,
389 we also expect to identify new therapeutic strategies in addition to understanding how existing
390 antimicrobials are impacted by hypoxic microenvironments known to exist *in vivo*. Finally, while we
391 use an airway-derived bacterial community and *F. nucleatum* as our model organisms, this work
392 motivates additional studies of the gut, lung, oral cavity, and other sites of infection, where etiological
393 roles of anaerobes have been proposed but specific pathogenic mechanisms remain unclear.

394

395 **ACKNOWLEDGEMENTS**

396 We thank the University of Minnesota Fabrication Shop for the custom design of our anaerobic
397 chamber culture manifold. We are also grateful for Emma Stanley (10X Genomics) and Jerry Daniel
398 at the University of Minnesota Genomics Center who provided assistance with scRNAseq. This work
399 was supported by the National Heart Lung and Blood Institute (HL136919), Cystic Fibrosis
400 Postdoctoral Fellowships to P.J.M. and J.R.F. (MOORE20F0, FLETC22F0), a National Institutes of
401 Health fellowship (#T90DE0227232) awarded through the National Institute of Dental and
402 Craniofacial Research to S.K.L., and an American Society for Microbiology Undergraduate Research
403 Fellowship to L.A.K..

404 **AUTHOR CONTRIBUTIONS**

405 P.J.M. and R.C.H. were responsible for study design and wrote the manuscript. P.J.M. T.D.W.,
406 L.A.K., S.J.A., S.K.L., J.R.F., and R.C.H., collected and analyzed the data and edited the manuscript.
407 T.D.W., S.J.A., and S.K.L. processed and analyzed RNA sequencing data. S.M.O. contributed cell
408 lines and assisted with experiments.

409

410 **DECLARATION OF INTERESTS**

411 The authors declare no competing interests.

412

413 **STAR METHODS**

414 **Epithelial Cell Culture**

415 Calu-3 cells were maintained in Minimal Essential Medium (Corning, USA) in 10% fetal
416 bovine serum (FBS, Gene) supplemented with 100 U/mL penicillin and 100 μg/mL streptomycin
417 (Gibco) at 37°C in a 5% CO_2 incubator. Upon reaching 80% confluency, 1 x 10^5 cells were passaged
418 onto 6.5mm culture inserts (24-well hanging inserts, 0.4 μm pore; Corning). When cells reached
419 confluency (~5 days), apical medium was removed to establish an air-liquid interface (ALI). Polarized
420 cells were maintained for an additional 21-28 days, with basolateral media changes every other day,
421 to facilitate differentiation and mucus accumulation.

422 Cell cultures were then assembled in a gas permeable multi-well plate manifold (**Fig. S2**).
423 Briefly, once polarized, Calu-3 cells were placed into gaskets in a 24-well gas-permeable plate
424 (CoyLabs, Grass Lake, MI) containing 800μl of MEM per well. Mineral oil (400μL) was added to
425 unused wells to prevent gas permeation from the basolateral to apical side of the manifold. Once
426 assembled and covered with a sterilized lid, the apparatus was moved to an anaerobic chamber
427 (90% N_2/5% H2/5% CO_2) while mixed gas (21% O_2/5% CO_2/74% N_2) was delivered to the base of
428 the plate to oxygenate the basolateral side of the polarized monolayer. A schematic of this workflow
429 is summarized in **Fig. S1**.

430 RPMI 2650 cells were similarly cultured, except Dulbecco's Modified Eagle Medium (DMEM)
431 was used as the basal growth medium. Primary nHTBE cells (Lonza Bioscience, CC-2540S)

432 harvested from healthy individuals were expanded using Pneumacult-Ex Plus (Stem Cell
433 Technologies) prior to seeding on 24-well inserts. Cells were maintained at ALI for ~21 days in a
434 Pneumacult ALI growth medium (Stem Cell Technologies) at 37°C and 5% CO_2 in a humidified
435 incubator.

436 **Cell culture assays**

437 Calu-3 barrier integrity was determined by trans-epithelial electrical resistance (TEER)
438 measured with a Millicell-ERS2 Volt-Ohm meter (Millipore Sigma). Barrier integrity was further
439 assessed using the Human E-cadherin Quantikine enzyme-linked immunosorbent assay (ELISA) kit
440 (R&D Systems, Minneapolis, MN). Cells were washed with 100μl of PBS, absorbance was measured
441 at 450 nm using a BioTek Synergy H2 plate reader and concentrations of E-cadherin were
442 determined against a standard curve according to manufacturer's instructions. Tight junction
443 formation was assayed using immunofluorescence with an anti-zonula occludens (ZO)-1 monoclonal
444 antibody (Thermo). To do so, Calu-3 cultures on Transwell inserts were chemically fixed in 4%
445 paraformaldehyde (PFA) in phosphate-buffered saline (PBS) for 1h at room temperature. Cells were
446 blocked in 10% goat serum and 1% bovine serum albumin (Sigma) for 15 min. After blocking, cells
447 were incubated with human anti-mouse ZO-1 (AlexaFluor-488 conjugate; ThermoFisher)(5 μg/mL)
448 for 1h. Transwell membranes were washed, removed from the supporting plastic insert, and mounted
449 on glass slides using Vectashield anti-fade mounting medium. Labeled cells were visualized (ex.
450 480nm, em. 525nm) on an Olympus IX83 inverted fluorescence microscope using a 20X objective
451 lens (0.75 NA). Finally, cytotoxicity was determined by lactate dehydrogenase (LDH) measurements
452 on cell-free supernatants collected from the apical compartment by washing with 100μL of PBS. LDH
453 was quantified using the Cytotoxicity Detection Kit Plus assay (Roche) according to manufacturer's
454 instructions. Data were calculated as percent LDH release compared with a lysed control and
455 reported as %LDH release = [(experimental value - low control)/(high control-low control)] x 100.

456 **Immunoassays**

457 The inflammatory response of Calu-3 cells was measured after 24h of culture in the anaerobic
458 chamber. To do so, spent medium was collected from the apical side of Transwell cultures, and
459 interleukin (IL-) 8 and IL-6 were then measured by ELISA per manufacturer instructions (R&D

460 systems). Untreated epithelial cells grown under standard incubator conditions (5% CO_2) were used
461 as a control.

462 **FPLC**

463 Secreted mucins were collected from Calu-3 cells as previously described[24]. Briefly, cells
464 grown on Transwell inserts were solubilized in a reduction buffer consisting of 6M guanidine
465 hydrochloride, 0.1M Tris-HCl buffer, and 5mM EDTA (pH 8). Prior to solubilization, 10mM
466 dithiothreitol (DTT) and a cOmplete Mini protease inhibitor tablet (Roche) were added to 400mL of
467 reduction buffer to minimize mucin degradation. Cell suspensions were gently agitated by pipetting
468 to dislodge biomass, and each of the six Transwell suspensions per plate were pooled into a single
469 aliquot. Cells were rinsed with a reduction buffer to remove residual mucin. This mixture was then
470 incubated for 5h at 37°C, followed by the addition of 25 mM iodoacetamide and incubation overnight
471 at room temperature. Mucins were then dialyzed (1000 kDa MWCO) against 1L of 4M GuHCl buffer
472 containing 2.25 mM NaH_2PO_4-H_2O and 76.8 mM Na_2HPO_4 and proceeded for 36h with buffer
473 exchanges every 12h.

474 Fast protein liquid chromatography (FPLC) size-exclusion chromatography was then used to
475 evaluate the integrity of high-molecular weight mucins. Using an Akta Pure FPLC (GE Healthcare
476 BioSciences, Marlborough, MA) housed at 4°C, 500 μL of purified mucin was manually injected and
477 subjected to an isocratic run at a flow rate of 0.4 mL/min for 1.5 column volumes (CV) with 150mM
478 NaCl in 50 mM phosphate buffer (pH 7.2) on a 15mL 10/200 Tricorn column packed with Sepharose
479 4B-CL beads. Data were collected using Unicorn 7 software (GE Healthcare Biosciences).

480 **Bacterial strains and culture conditions**

481 *P. aeruginosa* PA14 was routinely cultured on Luria Bertani (LB) medium. *P. melaninogenica*
482 ATCC 25845, *S. parasanguinis* ATCC15912, *V. parvula* ATCC10790, and *Fusobacterium nucleatum*
483 *subsp. nucleatum* ATCC 25586 were obtained from Microbiologics (St. Cloud, MN). *S. gordonii* was
484 obtained from M.C. Herzberg (University of Minnesota) and *P. oris* 12252T was purchased from the
485 Japan Collection of Microorganisms. All anaerobes were maintained on Brain-Heart Infusion medium
486 supplemented with hemin (0.25 g/L), vitamin K (0.025 g/L) and laked sheep's blood (5% vol/vol)
487 (BHI-HKB) in an anaerobic chamber. A mucin-enriched anaerobic bacterial community (ABC)

488 derived from an individual with chronic rhinosinusitis was also used and was cultured in a minimal
489 mucin medium (MMM)[14,15]. Community composition was determined using 16S rRNA gene
490 sequencing as described previously [15].

491 **Bacterial challenge and infection**

492 Forty-eight hours prior to bacterial challenge, Calu-3 cells were incubated in MEM + FBS
493 without antibiotics. On the day of bacterial challenge, Transwells were assembled in the gas
494 permeable culture system and transferred into the anaerobic chamber where they were equilibrated
495 for 3h. Overnight cultures of each anaerobe and the anaerobic bacterial community (ABC) were
496 grown in MMM. Each individual culture was diluted to a concentration of ~1 x 10^6 colony forming
497 units (CFU) in MEM and 10 μL of bacterial suspension was added to the apical side of the Calu-3
498 cells. Similarly, 10 μL of an adjusted suspension (OD600nm = 0.1, ~8 x 10^6 CFUs) of the anaerobic
499 community was added to separate wells. Co-cultures were then incubated for an additional 24h.
500 Following anaerobe challenge, spent medium was collected and analyzed for cytotoxicity using the
501 LDH colorimetric assay (described above). Mucins were also collected as described above for
502 integrity analysis via FPLC. In a separate experiment, anaerobe viability was determined using plate
503 enumeration. Briefly, Calu-3 cells were washed with 100μL of PBS (to remove loosely bound cells)
504 or 0.25% Triton X-100 (to recover tightly bound or intracellular bacteria). Resulting washes were
505 serially diluted and plated on BHI or Laked Brucella Blood Agar (BBA) with Kanamycin (100 μg/mL)
506 and Vancomycin (7.5 μg/mL) for enumeration. The latter was used as the selective agents prevent
507 growth of most obligate Gram-negative and Gram-positive anaerobic bacteria, including most
508 facultative anaerobes.

509 For the *P. aeruginosa* colonization assay, Calu-3 cultures were removed from the anaerobic
510 chamber following anaerobe challenge. Cells were gently washed with PBS and subsequently
511 infected with 5 x 10^7 CFU of *P. aeruginosa* for 2h. After incubation, cells were gently washed three
512 times with PBS to remove unbound *P. aeruginosa* and were permeabilized using 0.25% Triton X-
513 100. Bacteria were enumerated by plating serial dilutions of Calu-3 cell lysates on LB agar. All assays
514 were performed using three biological replicates and data are reported as the mean of three
515 experiments.

516 **Bulk RNA sequencing**

517 The transcriptomic response of Calu-3 cells to anoxic culture and anaerobe challenge was
518 determined using RNAseq. Calu-3 cells were cultured at ALI as described above and harvested after
519 24h of (i) normoxic growth without bacterial challenge, (ii) DOAC growth without bacterial challenge,
520 and (iii) DOAC growth with anaerobic bacterial challenge. Normoxic, unchallenged cells were
521 maintained under standard incubator conditions. At the conclusion of each experiment, RNAlater
522 (Invitrogen) was added to the apical and basolateral side of each well. For each condition, RNA was
523 isolated from at least 5 separate Transwells using the RNeasy Micro Plus kit (Qiagen) according to
524 manufacturer's instructions. DNase treatment was performed as part of the RNA Clean and
525 Concentrator kit (Zymo). RNA quality (RIN > 9.7) and quantity were assessed using an Agilent
526 Bioanalyzer and RiboGreen, respectively. cDNA libraries were prepared using the SMARTer
527 Universal Low Input RNA Kit (Takara Bio) and submitted for sequencing at the University of
528 Minnesota Genomics Center on the Illumina NovaSeq 6000 platform.

529 The Ensembl GTF annotation file was filtered to remove annotations for non-protein-coding
530 features. Fastq files were evenly subsampled down to a maximum of 100,000 reads per sample.
531 Data quality in fastq files was assessed with FastQC. Raw reads were mapped to reference Human
532 (Homo_sapiens) genome assembly "GRCh38" using annotation from Ensembl release 98. Gene
533 counts were generated with 'featureCounts' of the RSubread package[79]. DESeq2/1.28.1 was used
534 to estimate size factors to generate normalized count data, estimate gene-wise dispersions, shrink
535 estimates using type='ashr', and perform Wald hypothesis testing [48,80]. Genes with a $\log_2$ fold-change
536 greater than 1 and Benjamini-Hochberg adjusted p-value < 0.001 were considered significant. Code
537 and data files are shared at https://github.com/Hunter-Lab-UMN/Moore_PJ_2022 and NCBI Gene
538 Expression Omnibus (GEO) Accession #GSE21824.

539 **Scanning electron microscopy**

540 Co-cultures were washed three times in 0.2M sodium cacodylate buffer and submerged in
541 primary fixative (0.15 M sodium cacodylate buffer, pH 7.4, 2% paraformaldehyde, 2%
542 glutaraldehyde, 4% sucrose, 0.15% alcian blue 8GX) for 22h. Transwell membranes were washed
543 three more times prior to a 90-minute treatment with secondary fixative (1% osmium tetroxide, 1.5%

544 potassium ferrocyanide, 0.135M sodium cacodylate, pH 7.4). After three final washes, cells were
545 dehydrated in a graded ethanol series (25%, 50%, 75%, 85%, 2 x 95%, and 2 x 100%) for 10 minutes
546 each before CO_2-based critical point drying. Transwell membranes were attached to SEM specimen
547 mounts using carbon conductive adhesive tape and sputter coated with ~5 nm iridium using the Leica
548 ACE 600 magnetron-based system. Cells were imaged using a Hitachi S-4700 field emission SEM
549 with an operating voltage of 2kV. Images were false colored using Adobe Photoshop CS6.

550 **Single cell RNA sequencing and analysis.**

551 nHTBE cells grown on Transwell inserts were incubated in antibiotic-free Pneumocult
552 medium for 48h prior to bacterial challenge. nHTBEs were assembled in the DOAC system and
553 transferred into the anaerobic chamber. After 3 hours of nHTBE equilibration, an overnight culture
554 of *F. nucleatum subsp. nucleatum* ATCC 25586 grown in BHI was diluted to a concentration of 1 x
555 10^6 CFU in Pneumacult medium and 10 μL of bacterial suspension was added to the apical side of
556 the nHTBE cells in the anaerobic chamber. Co-cultures were incubated for 24 h prior to epithelial
557 cell homogenization and cell capture.

558 Samples were prepared for scRNAseq as described previously[40]. Briefly, single cell
559 suspensions were washed with PBS + 5% FBS, resuspended in 200μL of PBS + 5% FBS, passed
560 through a 70 μm cell strainer, and placed on ice. Cells were counted using trypan blue on a BioRad
561 TC20 automated cell counter. A targeted cell input of 5,000 cells per condition were used to generate
562 Gel Bead-In Emulsion (GEMs). The Chromium Next GEM Single Cell 3' Gel beads v3.1 kit (10X
563 Genomics, Pleasanton, CA) was used to create GEMS following manufacturer's instructions.
564 Captured GEMS were used for cDNA synthesis and library preparation using the Chromium Single
565 Cell 3' Library Kit v3.1, followed by sequencing using the Illumina NovaSeq platform.

566 Raw count matrices were generated with Cell Ranger (v.3.0.1) for alignment to the human
567 reference genome (Homo_sapiens.GRCh38). The resulting raw count matrix for each experimental
568 data set was imported into an R pipeline using Seurat (v. 4.1.0)[81] for quality control, normalization,
569 integration, clustering, and differential expression analysis. Data were filtered to remove low quality
570 cells using the following criteria: number of UMI counts per cell ≥ 500, number of genes per cell ≥
571 250, number of genes detected per UMI ≥ 0.8, mitochondrial ratio less than 0.25, and genes

572 expressed in ≥ 10 cells. '*SCTransform*' was used to normalize the data and regress out variation due
573 to mitochondrial gene expression. Cells were integrated across conditions using default parameters
574 except all 300 most variable genes identified by *SCTransform* were used. Cell clustering was
575 performed based on the first 20 principal components using the *FindClusters* function with a 0.4
576 resolution. Conserved markers in each cluster were identified using *FindConservedMarkers*. Cell
577 types for each cluster were then identified using the top 10 markers by average log fold change
578 across groups. This list of top markers was compared to known cell markers for basal cells, secretory
579 cells, ciliated cells, and ionocytes (Plasschaert). Clusters with a minimum of two out of the ten top
580 markers corresponding to a particular cell type were labelled as such. DESeq2 (v. 1.34.0) was then
581 used to perform pseudobulk differential expression analysis across the different cell types accounting
582 for *F. nucleatum* challenge. Specifically, this package was used to estimate size factors, normalized
583 count data, estimate gene-wise dispersions, shrink estimates using type='apeglm'[82], and perform
584 Wald hypothesis testing. Genes with a $\log_2$ fold-change greater than 1 and Benjamini-Hochberg
585 adjusted p-value < 0.05 were considered significant. Pattern recognition receptor gene expression
586 was visualized in the untreated population using Nebulosa (v.1.4.0) *plot_density* function. All code
587 and data files are shared at https://github.com/Hunter-Lab-UMN/Moore_PJ_2022.

588 **REFERENCES**

589 1. Segal, L. N., Alekseyenko, A. V., Clemente, J. C., Kulkarni, R., Wu, B., Gao, Z., Chen, H.,
590 Berger, K.I., Goldring, R.M., Rom, W.N., Blaser, M.J., and Weiden, M.D. (2013). Enrichment of
591 lung microbiome with supraglottic taxa is associated with increased pulmonary inflammation.
592 Microbiome **1**, 19.
593 2. Charlson, E.S., Bittinger, K., Haas, A.R., Fitzgerald, A.S., Frank, I., Yadav, A., Bushman, F.D.,
594 Collman, R.G. (2011). Topographical continuity of bacterial populations in the healthy human
595 respiratory tract. Am. J. Respir. Crit. Care Med. 184, 957-963.
596 3. Morris, A., Beck, J.M., Schloss, P.D., Campbell, T.B., Crothers, K., Curtis, J.L., Flores, S.C.,
597 Fontenot, A.P., Ghedin, E., Huang, L. et al. (2013). Comparison of the respiratory microbiome
598 in healthy nonsmokers and smokers. Am. J. Respir. Crit. Care Med. 187, 1067-1075.
599 4. Dickson, R.P., Erb-Downward, J.R., Freeman, C.M., McCloskey, L., Falkowski, N.R., Huffnagle,
600 G.B., Curtis, J.L. (2017). Bacterial topography of the healthy human lower respiratory tract. mBio
601 8, e02287-16.
602 5. Pragman, A.A., Kim, H.B., Reilly, C.S., Wendt, C., Isaacson, R.E. (2012) The lung microbiome
603 in moderate and severe chronic obstructive pulmonary disease. PLoS One 7, e47305.
604 6. Tunney, M.M., Field, T.R., Moriarty, T.F., Patrick, S., Doering, G., Muhlebach, M.S., Wolfgang,
605 M.C., Boucher, R., Gilpin, D.F., McDowell, A., Elborn, J.S. (2008). Detection of anaerobic
606 bacteria in high numbers in sputum from patients with cystic fibrosis. Am. J. Respir. Crit. Care
607 Med. 177, 995-1001.
608 7. Rogers, G.B., van der Gast, C.J., Cuthbertson, L., Thomson, S.K., Bruce, K.D., Martin, M.L.,
609 Serisier, D.J. (2013) Clinical measures of disease in adult non-CF bronchiectasis correlate with
610 airway microbiota composition. Thorax 68, 731-737.
611 8. Lucas, S.K., Yang, R., Dunitz, J.M., Boyer, H.C., Hunter, R.C. (2018) 16S rRNA gene
612 sequencing reveals site-specific signatures of the upper and lower airways of cystic fibrosis
613 patients. J. Cyst. Fibros. 17, 204-212.
614 9. Segal, L.N., Clemente, J.C., Li, Y., Ruan, C., Cao, J., Danckers, M., Morris, A., Tapyrik, S., Wu,
615 B.G., Diaz, P., et al. (2017) Anaerobic bacterial fermentation products increase tuberculosis risk
616 in antiretroviral-drug-treated HIV patients. *Cell Host Microbe* **21**, 530-537.
617 10. Marik, P., and Careau, P. (1999). The role of anaerobes in patients with ventilator-associated
618 pneumonia and aspiration pneumonia: A prospective study. Chest 115, 178-183.
619 11. Sulaiman, I., Wu, B.G., Li, Y., Scott, A.S., Malecha, P., Scaglione, B., Wang, J., Basavaraj, A.,
620 Chung, S., Bantis, K. et al. (2018). Evaluation of the airway microbiome in nontuberculous
621 mycobacteria disease. Eur. Respir. J. 52, 1800810.
622 12. Mirković, B., Murray, M.A., Lavelle, G.M., Molloy, K., Azim, A.A., Gunaratnam, C., Healy, F.,
623 Slattery, D., McNally, P., Hatch, J. et al. (2015). The role of short-chain fatty acids, produced by
624 anaerobic bacteria, in the cystic fibrosis airway. Am. J. Respir. Crit. Care Med. 192, 1314-1324.

625 13. Ghorbani, P., Santhakumar, P., Hu, Q., Djiadeu, P., Wolever, T.M., Palaniyar, N., Grasemann,
626 H. (2015). Short-chain fatty acids affect cystic fibrosis airway inflammation and bacterial growth.
627 Eur. Respir. J. 46, 1033-1045.
628 14. Flynn, J.M., Niccum, D., Dunitz, J.M., Hunter, R.C. (2016) Evidence and role for bacterial mucin
629 degradation in cystic fibrosis airway disease. PLoS Pathog. 12, e1005846.
630 15. Lucas, S.K., Villareal, A.R., Ahmad, M.M., Itabiyi, A., Feddema, E., Boyer, H.C., Hunter, R.C.
631 (2021). Anaerobic microbiota derived from the upper airways impact *Staphylococcus aureus*
632 physiology. Infect. Immun. 89, e00153-21.
633 16. Muhlebach, M.S., Hatch, J.E., Einarsson, G.G., McGrath, S.J., Gilpin, D.F., Lavelle, G., Mirkovic,
634 B., Murray, M.A., McNally, P., Gotman, N. et al. (2018) Anaerobic bacteria cultured from cystic
635 fibrosis airways correlate to milder disease: a multisite study. Eur. Resp. J. 52, 1800242.
636 17. Carmody, L.A., Caverly, L.J., Foster, B.K., Rogers, M.A.M., Kalikin, L.H., Simon, R.H.,
637 VanDevanter, D.R., LiPuma, J.J. (2018). Fluctuations in airway bacterial communities
638 associated with clinical states and disease stages in cystic fibrosis. PLoS One 13, e0194060
639 (2018).
640 18. Hendricks, M.R., Lashua, L.P., Fischer, D.K., Flitter, B.A., Eichinger, K.M., Durbin, J.E., Sarkar,
641 S.N., Coyne, C.B., Empey, K.M., Bomberger, J.M. (2016). Respiratory syncytial virus infection
642 enhances *Pseudomonas aeruginosa* biofilm growth through dysregulation of nutritional
643 immunity. Proc. Nat. Acad. Sci. U. S. A. 113, 1642-1647.
644 19. Moreau-Marquis, S., Bomberger, J.M., Anderson, G.G., Swiatecka-Urban, A., Ye, S., O'Toole,
645 G.A., Stanton, B.A. (2008). The DeltaF508-CFTR mutation results in increased biofilm formation
646 by *Pseudomonas aeruginosa* by increasing iron availability. Am. J. Physiol. Lung Cell. Mol.
647 Physiol. 295, L25-37.
648 20. M.R. Kiedrowski, M. R. *et al.* Biofilm Growth on Cystic Fibrosis Airway Epithelial Cells Is
649 Enhanced during Respiratory Syncytial Virus Coinfection. *mSphere* **3**,
650 doi:10.1128/mSphere.00341-18 (2018).
651 21. Aeneas, K., Fledelius Rickelt, L., Johansen, H.K., von Buchwald, C., Pressler, T., Hoiby, N.,
652 Jensen, P.O. (2011). Decreased mucosal oxygen tension in the maxillary sinuses in patients
653 with cystic fibrosis. J Cyst Fib 10, 114-120.
654 22. Cowley, E.S., Kopf, S.H., LaRiviere, A., Ziebis, W., Newman, D.K. (2015). Pediatric cystic fibrosis
655 sputum can be chemically dynamic, anoxic, and extremely reduced due to hydrogen sulfide
656 formation. mBio **6,** e00767-15.
657 23. Han, Y. (2015) *Fusobacterium nucleatum:* a commensal-turned pathogen. Curr. Op. Microbiol.
658 23, 141-147.
659 24. Evert, C., Loesekann, T., Bhat, G., Shajahan, A., Sonon, R., Azadi, P., Hunter, R.C. (2019).
660 Generation of 13C-labeled MUC5AC mucin oligosaccharides for stable isotope probing of host-
661 associated microbial communities. ACS Infect. Dis. 5, 385-393.

662 25. Tamm, M., Bihl, M., Eickelberg, O., Stulz, P., Perruchoud, A.P., Roth, M. (1998). Hypoxia-
663 induced interleukin-6 and interleukin-8 production is mediated by platelet-activating factor and
664 platelet-derived growth factor in primary human lung cells. Am. J. Respir. Cell Mol. Biol. 19, 653-
665 661.
666 26. Kiedrowski, M.R., A.E. Paharik, L.W. Ackermann, A.U. Shelton, S.B. Singh, T.D. Starner, A.R.
667 Horswill. (2016). Development of an *in vitro* colonization model to investigate *Staphylococcus*
668 *aureus* interactions with airway epithelia. Cell. Microbiol. 18, 720-732.
669 27. Liu, Y.C., Hussain, F., Negm, O., Paiva, A.C., Halliday, N., Dubern, J.F., Singh, S., Muntaka, S.,
670 Wheldon, L., Luckett, J., Tighe, P. et al. (2018). Contribution of the alkylquinolone quorum
671 sensing system to the interaction of *Pseudomonas aeruginosa* with bronchial epithelial cells.
672 Front. Microbiol. 9, 3018.
673 28. Hayashi, J., Saito, I., Ishikawa, I., Miyasaka, N. (1994) Effects of cytokines and periodontopathic
674 bacteria on the leukocyte function-associated antigen 1/intracellular adhesion molecular 1
675 pathway in gingival fibroblasts in adult periodontitis. Infect. Immun. 62, 5205-5212.
676 29. Jia, L., Shi, Y., Wen, Y., Li, W., Feng, J., Chen, C. (2018). The roles of TNFAIP2 in cancers and
677 infectious diseases. J. Cell. Mol. Med. 22, 5188-5195.
678 30. De Filippo, K., Dudeck, A., Hasenberg, M., Nye, E., van Rooijen, N., Hartmann, K., Gunzer, M.,
679 Roers, A., Hogg, N. (2013). Mast cell and macrophage chemokines CXCL1/CXCL2 control the
680 early stage of neutrophil recruitment during tissue inflammation. Blood 121, 4930-4937.
681 31. Koltsova, E.K., Ley, K. (2010) The mysterious ways of the chemokine CXCL5. Immunity 33, 7-
682 9.
683 32. Peterman, E.M., Sullivan, C., Goody, M.F., Rodriguez-Nunez, I., Yoder, J.A., Kim, C.H. (2015).
684 Neutralization of mitochondrial superoxide by superoxide dismutase 2 promotes bacterial
685 clearance and regulates phagocyte numbers in zebrafish. Infect. Immun. 83, 430-440.
686 33. Sallenave, J.M., Cunningham, G.A., James, R.M., McLachlan, G., Haslett, C. (2003) Regulation
687 of pulmonary and systemic bacterial lipopolysaccharide responses in transgenic mice
688 expressing human elafin. Infect. Immun. 71, 3766-3774.
689 34. Henderson, A.G., Ehre, C., Button, B., Abdullah, L.H., Cai, L.H., Leigh, M.W., DeMaria, G.C.,
690 Matsui, H., Donaldson, S.H., Davis, C.W., Sheehan, J.K., Boucher, R.C., Kesimer, M. (2014).
691 Cystic fibrosis airway secretions exhibit mucin hyperconcentration and increased osmotic
692 pressure. J. Clin. Invest. 124, 3047-3060.
693 35. Audry, M., Robbe-Masselot, C., Barnier, J.P., Gachet, B., Saubaméa, B., Schmitt, A.,
694 Schönherr-Hellec, S., Léonard, R., Nassif, X., Coureuil, M. (2019). Airway mucus restricts
695 neisseria meningitidis away from nasopharyngeal epithelial cells and protects the mucosa from
696 inflammation. mSphere 4, e00494-19.
697 36. Ulrich, M., Beer, I., Braitmaier, P., Dierkes, M., Kummer, F., Krismer, B., Schumacher, U.,
698 Gräpler-Mainka, U., Riethmüller, J., Jensen, P.Ø. et al. (2010). Relative contribution of

699 *Prevotella intermedia* and *Pseudomonas aeruginosa* to lung pathology in airways of patients
700 with cystic fibrosis. Thorax 65, 978-984.
701 37. Plasschaert, L.W., Zilionis, R., Choo-Wing, R., Savova, V., Knehr, J., Roma, G., Klein, A.M.,
702 Jaffe, A.B. (2018). A single cell atlas of the tracheal epithelium reveals the CFTR-rich pulmonary
703 ionocyte. Nature 560, 377-381.
704 38. Kim, N., Kim, H.K., Lee, K., Hong, Y., Cho, J.H., Choi, J.W., Lee, J.I., Suh, Y.L., Ku, B.M., Eum,
705 H.H., Choi, S. (2020). Single-cell RNA sequencing demonstrates the molecular and cellular
706 reprogramming of metastatic lung adenocarcinoma. Nat. Comm. 11, 1-5.
707 39. Schupp, J., Khanal, S., Gomez, J.L., Sauler, M., Adams, T.S., Chupp, G.L., Yan, X., Poli, S.,
708 Zhao, Y., Montgomery, R.R., et al. (2020). Single-cell transcriptional archetypes of airway
709 inflammation in cystic fibrosis. Am. J. Respir. Crit. Care Med. 202, 1419-1429.
710 40. Fiege, J.K., Thiede, J.M., Nanda, H.A., Matchett, W.E., Moore, P.J., Montanari, N.R., Thielen,
711 B.K., Daniel, J., Stanley, E., Hunter, R.C.,et al. (2021). PLoS Pathogens 17, e1009292.
712 41. Edwards, J.A., Groathouse, N.A., Boitano, S. (2005). *Bordetella bronchiseptica* adherence to
713 cilia is mediated by multiple adhesin factors and blocked by surfactant protein A. Infect Immun.
714 73, 3618-26.
715 42. Franklin, A.L., Todd, T.O.M., Gurman, G., Black, D., Mankinen-Irvin, P.M., Irvin, R.T. (1987).
716 Adherence of *Pseudomonas aeruginosa* to cilia of human tracheal epithelial cells. Infect. Immun.
717 55,1523-5.
718 43. Niederman, M.S., Rafferty, T.D., Sasaki, C.T., Merrill, W.W., Matthay, R.A., Reynolds, H.Y.
719 (1983). Comparison of bacterial adherence to ciliated and squamous epithelial cells obtained
720 from the human respiratory tract. Am. Rev. Respir. Dis. 127,85-90.
721 44. Trapnell, C., Cacchiarelli, D., Grimsby, J., Pokharel, P., Li, S., Morse, M., Lennon, N.J., Livak,
722 K.J., Mikkelsen, T.S., Rinn, J.L. (2014). The dynamics and regulators of cell fate decisions are
723 revealed by pseudotemporal ordering of single cells. Nat. Biotechnol. 32,381-386.
724 45. Cao, J., Spielmann, M., Qiu, X., Huang, X., Ibrahim, D.M., Hill, A.J., Zhang, F., Mundlos, S.,
725 Christiansen, L., Steemers, F.J., Trapnell, C. (2019). The single-cell transcriptional landscape
726 of mammalian organogenesis. Nature. 566, 496-502.
727 46. Greene, C.M., McElvaney, N.G. (2005) Toll-like receptor expression and function in airway
728 epithelial cells. Arch. Immunol. 53, 418-427.
729 47. Opitz, B., van Laak, V., Eitel, J., Suttorp, N. (2010). Innate immune recognition in infectious and
730 noninfectious diseases of the lung. Am. J. Respir. Crit. Care Med. 181, 1294-1309.
731 48. Love, M., Huber, W., Anders, S. (2014). Moderated estimation of fold change and dispersion for
732 RNA-seq data with DESeq2. Genome Biol. 15, 550.
733 49. Engevik, M., Danhof, H.A., Ruan, W., Engevik, A.C., Chang-Graham, A.L., Engevik, K.A., Shi,
734 Z., Zhao, Y., Brand, C.K., Krystofiak, E.S., Venable, S. (2021). *Fusobacterium nucleatum*
735 secretes outer membrane vesicles and promotes intestinal inflammation. mBio 12, e02706-20.

736 50. Kostic, A.D., Chun, E., Robertson, L., Glickman, J.N., Gallini, C.A., Michaud, M, Clancy, T.E.,
737 Chung, D.C., Lochhead, P., Hold, G.L. et al. (2013) *Fusobacterium nucleatum* potentiates
738 intestinal tumorigenesis and modulates the tumor-immune microenvironment. Cell Host Microbe
739 14, 207-215.
740 51. Han, Y.W., Redline, R.W., Li, M., Yin, L., Hill, G.B., McCormick, T.S. (2004). *Fusobacterium*
741 *nucleatum* induces premature and term stillbirths in pregnant mice: implication of oral bacterial
742 in preterm birth. Infect. Immun. 72, 2272-2279.
743 52. Williams, M.D., Kerber, C.A., Tergin, H.F. (2013). Unusual presentation of Lemierre's syndrome
744 due to *Fusobacterium nucleatum.* J. Clin. Microbiol. 41, 3445-3448.
745 53. Roos, P.H., Bolt, H.M. (2005). Cytochrome P450 interactions in human cancers: new aspects
746 considering CYP1B1. Exp. Op. Drug. Metab. Toxicol. 1, 187-202.
747 54. Wang, W., Liu, F., Wang, C., Wang, C., Tang, Y., Jiang, Z. (2017). Glutathione S-transferase A1
748 mediates nicotine-induced lung cancer cell metastasis by promoting epithelial-mesenchymal
749 transition. Exp. Ther. Med. 14, 1783-1788.
750 55. Chen, Q., Wu, K., Qin, X., Yu, Y., Wang, X., Wei, K. (2020). LASP1 promotes proliferation,
751 metastasis, invasion in head and neck squamous cell carcinoma and through direct interaction
752 with HSPA1A. J. Cell. Mol. Med. 24, 1626-1629.
753 56. Tsay, J.J., Wu, B., Badri, M., Clemente, J.C., Shen, N., Meyn, P., Li, Y., Yie, T.A. et al. (2018).
754 Airway microbiota is associated with upregulation of the PI3K pathway in lung cancer. Am. J.
755 Respir. Crit. Care Med. 198,1188-1198.
756 57. Tsay, J.J., Wu, B.G., Sulaiman, I., Gershner, K., Schluger, R., Li, Y., Yie, T.A., Meyn, P., Olsen,
757 E., Perez, L., Franca, B. et al. (2021). Lower airway dysbiosis affects lung cancer progression.
758 Cancer Disc 11:293-307.
759 58. Chu, S., Cheng, Z., Yin, Z., Xu, J., Wu, F., Jin, Y., Yang, G. (2022). Airway *Fusobacterium* is
760 associated with poor resposne to immunotherapy in lung cancer. Onco. Targets Ther. 15:201-
761 213 (2022)
762 59. von Martels, J.Z.H, Sadaghian Sadabad, M., Bourgonje, A.R., Blokzijl, T., Dijkstra, G., Faber,
763 K.N., Harmsen, H.J.M. (2017). The role of gut microbiota in health and disease: In vitro modeling
764 of host-microbe interactions at the aerobe-anaerobe interphase of the human gut. Anaerobe 44,
765 3-12.
766 60. Yee, M., Kim, S., Sethi, P., Düzgüneş, N., Konopka, K. (2014) *Porphyromonas gingivalis*
767 stimulates IL-6 and IL-8 secretion in GMSM-K, HSC-3 and H413 oral epithelial cells. Anaerobe
768 28, 62-67.
769 61. Pinnock, A., Murdoch, C., Moharamzadeh, K., Whawell, S., Douglas, C.W.I. (2014).
770 Characterisation and optimisation of organotypic oral mucosal models to study *Porphyromonas*
771 *gingivalis* invasion. Microb. Infect 16, 310-319.

772 62. Han, Y.W., Shi, W., Huang, G.T., Kinder Haake, S., Park, Kuramitsu, H., Genco, R.J. (2000)
773 Interactions between periodontal bacteria and human oral epithelial cells: *Fusobacterium*
774 *nucleatum* adheres to and invades epithelial cells. Infect. Immun. 68, 3140-3146.
775 63. Gursoy, U.K., Könönen, E., Uitto, V.J. (2009). *Prevotella intermedia* ATCC 25611 targets host
776 cell lamellipodia in epithelial cell adhesion and invasion. Oral Microbiol. Immunol. 24, 304-309.
777 64. Shin, W., Wu, A., Massidda, M.W., Foster, C., Thomas, N., Lee, D.W., Koh, H., Ju, Y., Kim, J.,
778 Kim, H.J. (2019). A robust longitudinal co-culture of obligate anaerobic gut microbiome with
779 human intestinal epithelium in an anoxic-oxic interface-on-a-chip. Front. Bioeng. Biotechnol. 7,
780 13.
781 65. Marzorati, M., Vanhoecke, B., De Ryck, T., Sadaghian Sadabad, M., Pinheiro, I., Possemiers,
782 S., Van den Abbeele, P., Derycke, L., Bracke, M., Pieters, J. et al. (2014). The HMI™ module:
783 a new tool to study the host-microbiota interaction in the human gastrointestinal tract in vitro.
784 BMC Microbiol 14, 133.
785 66. Kim, H.J., Huh, D., Hamilton, G., Ingber, D.E. (2012). Human gut-on-a-chip inhabited by
786 microbial flora that experiences intestinal peristalsis-like motions and flow. Lab Chip 12, 2165-
787 2174.
788 67. Kim, H.J., Li, H., Collins, J.J., Ingber, D.E. (2018). Contributions of microbiome and mechanical
789 deformation to intestinal bacterial overgrowth and inflammation in a human gut-on-a-chip. Proc.
790 Nat. Acad. Sci. U. S. A. 113, E7-15.
791 68. Shah, P., Fritz, J.V., Glaab, E., Desai, M.S., Greenhalgh, K., Frachet, A., Niegowska, M., Estes,
792 M., Jäger, C., Seguin-Devaux, C., Zenhausern, F., Wilmes, P. (2016). A microfluidics-based *in*
793 *vitro* model of the gastrointestinal human-microbe interface. *Nat Commun* **7**, 11535.
794 69. Stewart, C.E., Torr, E.E., Mohd Jamili, N.H., Bosquillon, C., Sayers, I. (2012). Evaluation of
795 differentiated human bronchial epithelial cell culture systems for asthma research. J Allergy
796 2012, 943982.
797 70. Grainger, C.I., Greenwell, L.L., Lockley, D.J., Martin, G.P., Forbes, B. (2006) Culture of Calu-
798 3 cells at the air interface provides a representative model of the airway epithelial barrier. Pharm.
799 Res. 23, 1482-1490.
800 71. Singh, P.K., Schaefer, A.L., Parsek, M.R., Moninger, T.O., Welsh, M.J., Greenberg, E.P. (2000).
801 Quorum-sensing signals indicate that cystic fibrosis lungs are infected with bacterial biofilms.
802 Nature 407, 762-764.
803 72. Martens, K., Hellings, P.W., Steelant, B. (2018). Calu-3 epithelial cells exhibit different immune
804 and epithelial barrier responses from freshly isolated primary nasal epithelial cells in vitro. Clin.
805 Transl. Allergy 8, 40.
806 73. Moore, W.E., Moore, L.V. (2000). The bacteria of periodontal diseases. Periodont. 5:66-77.

807 74. Han, Y.W., Shen, T., Chung, P., Buhimschi, I.A., Buhimschi, C.S. (2009). Uncultivated bacteria
808 as etiologic agents of intra-amniotic inflammation leaading to pre-term birth. J. Clin. Microbiol.
809 47:38-47.
810 75. Rubenstein, M.R., Wang, X., Liu, W., Hao, Y., Cai, G., Han, Y.W. (2013). *Fusobacterium*
811 *nucleatum* promotes colorectal carcinogenesis by modulating E-cadherin / β-catenin signaling
812 via its FadA adhesin. Cell Host Microb. 14:195-206.
813 76. Tahara, T., Shibata, T., Kawamura, T., Okubo, M., Ichikawa, Y., Sumi, K., Miyata, M., Ishizuka,
814 T. et al. (2014). Fusobacterium detected in colonic biopsy and clinicopathological features of
815 ulcerative colitis in Japan. Dig. Dis. Sci. 60:205-210
816 77. Strauss, J., Kaplan, G.G., Beck, P.L., Rioux, K., Panaccione, R., Devinney, R., Lynch, T., Allen-
817 Vercoe, E. (2011) Invasive potential of gut mucosa-derived *Fusobacterium nucleatum* positively
818 correlates with IBD status of thet host. Inflamm. Bowel Dis. 17:1971-1978.
819 78. Alon-Maimon, T., Mandelboim, O., Bachrach, G. (2022). *Fusobacterium nucleatum* and cancer.
820 Periodontology. 89:166-180.
821 79. Liao, Y., Smyth, G.K., Shi, W. (2019). The R package Rsubread is easier, faster, cheaper,
822 and better for alignment and quantification of RNA sequencing reads. Nucleic Acids Res.
823 47, e47.
824 80. Stephens, M. (2017). False discovery rates: a new deal. Biostatistics. 18, 275-294.
825 81. Butler, A., Hoffman, P., Smibert, P., Papalexi, E., Satija, R. (2018). Integrating single-cell
826 transcriptomic data across different conditions, technologies, and species. Nat. Biotechnol.
827 36:411-420.
828 82. Zhu, A., Ibrahim, J.G., Love, M.I. (2019) Heavy-tailed prior distributions for sequence count data:
829 removing the noise and preserving large differences. Bioinformatics. 35:2084-2092.
830

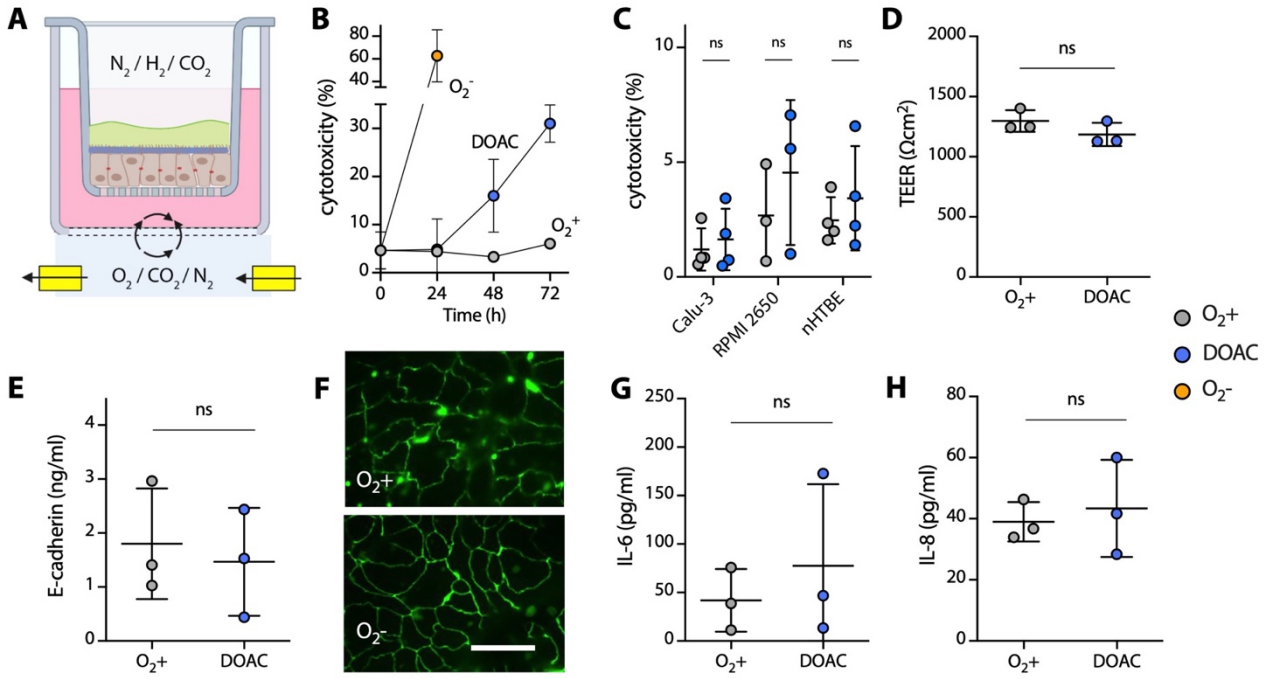

Fig. 1. Dual oxic-anoxic culture (DOAC) of human bronchial epithelial cells. (A) Primary and immortalized (Calu-3, RPMI2650) cells are cultured on Transwell inserts at ALI for 21-28 days, transferred to a gas permeable multi-well plate manifold in an anaerobic chamber, and incubated under dual oxic-anoxic culture conditions where the apical compartment is oxygen-limited and mixed gas is delivered basolaterally. Figure created with BioRender.com **(B)** Cytotoxicity as measured by lactate dehydrogenase (LDH) in the DOAC culture medium over time relative to normoxic (O_2^+)and strict anoxic (O_2^-) culture conditions. LDH activity is expressed as a % relative to normoxic cultures at t=0 and a lysed control culture. **(C)** LDH release by Calu-3, RPMI 2650, and primary nHTBE cells under normoxic (grey) and DOAC (blue) culture conditions after 24h. **(D)** Transepithelial electrical resistance (TEER), **(E)** E-cadherin concentrations, **(F)** immunofluorescence of zonula occludens 1 (ZO-1) tight junction proteins, and cytokines **(G)** IL-6, and **(H)** IL-8 showed no significant differences between normoxic and DOAC culture conditions after 24h. All data shown for panels B-D, F, and G were derived from at least three independent experiments with three technical replicates each and were compared using an unpaired t-test with Welch's correction. Images in panel F are representative of three independent experiments. Bar = 20μm.

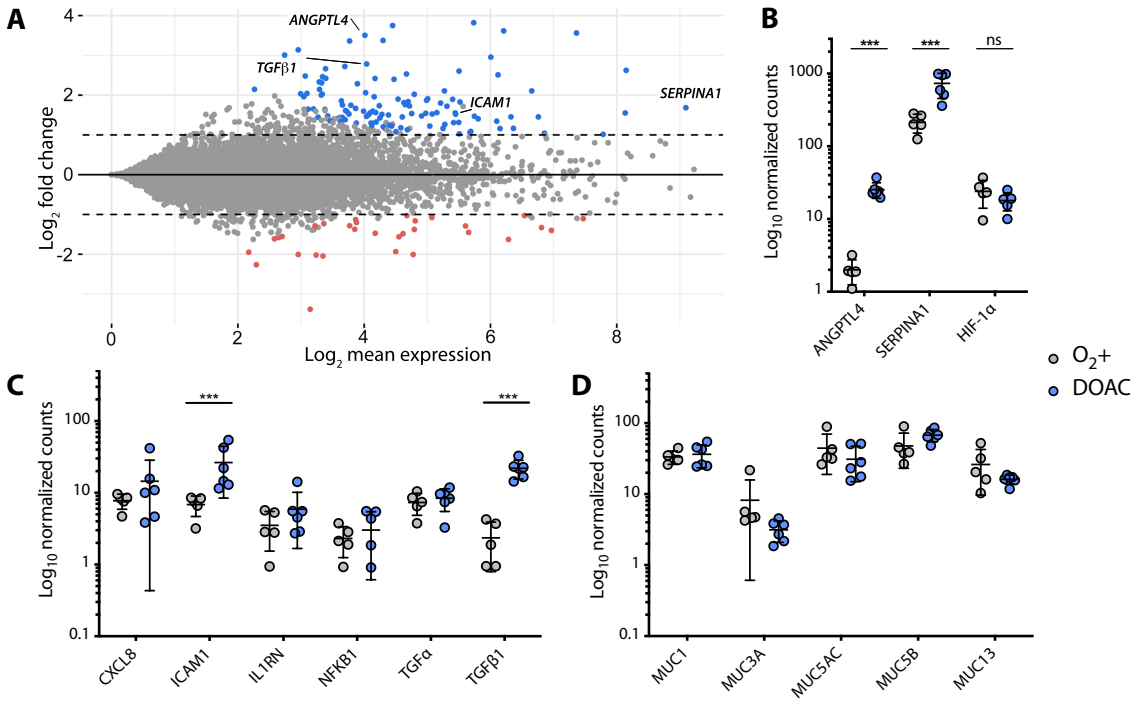

Fig. 2. **Dual oxic-anoxic culture of Calu-3 cells yields a similar transcriptomic profile to normoxic culture conditions (ALI). (A)** MA plot representation of Calu-3 gene expression under DOAC conditions relative to normoxic culture at ALI (117 upregulated, 31 downregulated, log2fc > 1, padj <0.001). **(B)** *ANGPTL4* and *SERPINA1* were differentially expressed, though HIF-1α was consistent between cultures. Few changes in **(C)** inflammatory biomarkers and **(D)** mucin gene expression were observed. Data shown in panels B-D are $\log_{10}$-normalized gene counts from five or six independent biological replicates and were compared using the Wald test, Benjamini-Hochberg adjusted (***, p<0.001).

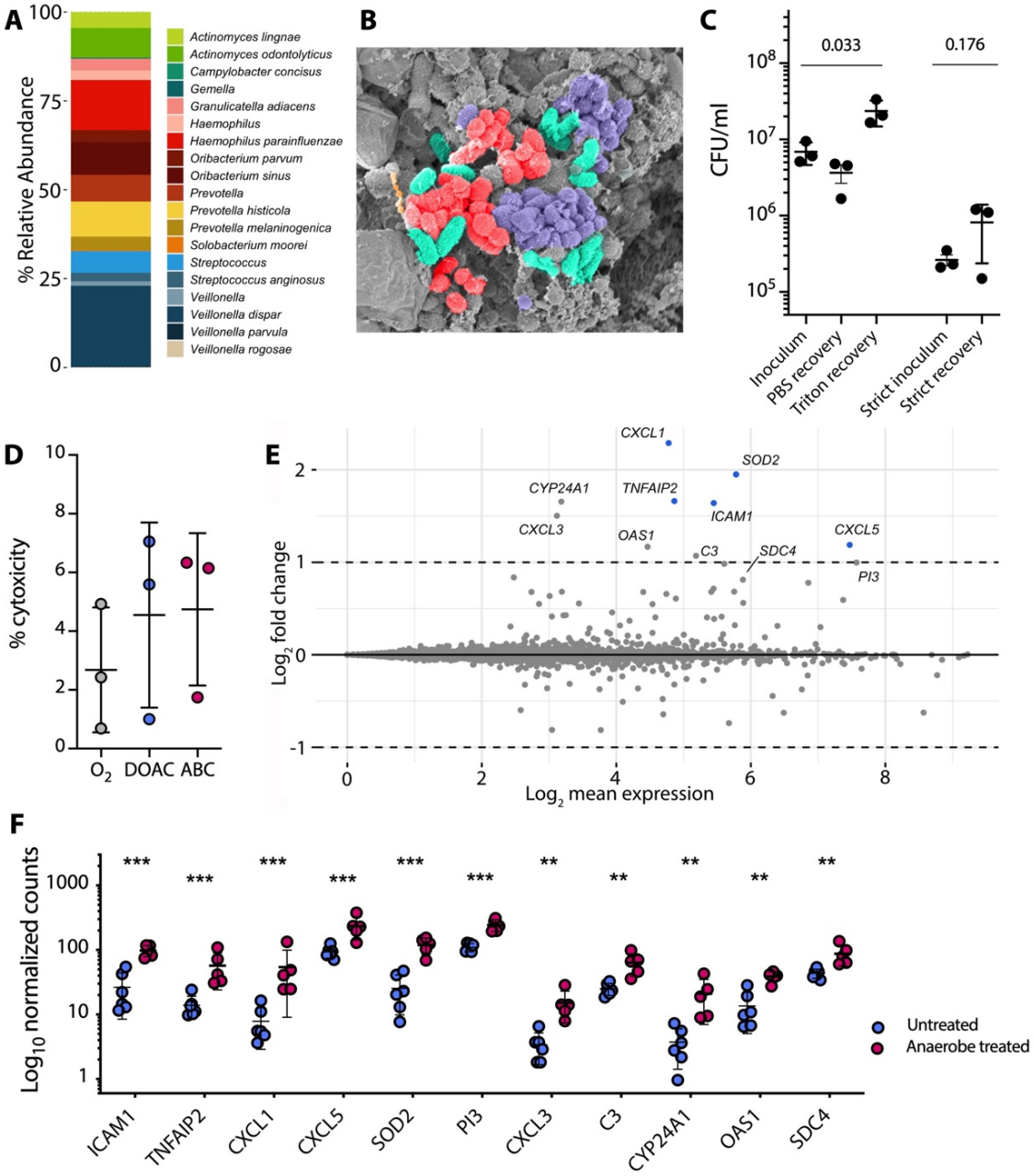

Fig. 3. Anaerobic microbiota colonize the apical surface of Calu-3 cells and induce a pro-inflammatory response. (A) Taxonomic composition of an enriched anaerobic bacterial consortium (ABC) derived from the upper airways. **(B)** SEM micrograph of Calu-3 cells after challenge with ABC. **(C)** Bacterial recovery from Calu-3 cells after 24h by washing with PBS and TritonX-100. Strict anaerobe CFUs were determined by plate enumeration on Brucella Blood Agar under anoxic conditions. **(D)** Anaerobe (ABC) challenge did not result in Calu-3 cytotoxicity relative to unchallenged cells grown aerobically (O_2) or under dual oxic-anoxic conditions (DOAC). **(E)** MA plot representation of Calu-3 gene expression under DOAC after ABC challenge relative to an untreated DOAC control. **(F)** Log_{10}-normalized gene counts from five or six independent biological replicates. Data in panels C and D were compared using a one-way ANOVA with Dunn's multiple comparisons test (n=3). Data in panels E and F were compared using a Wald test, Benjamini-Hochberg adjusted (***p<0.001, **<0.01).

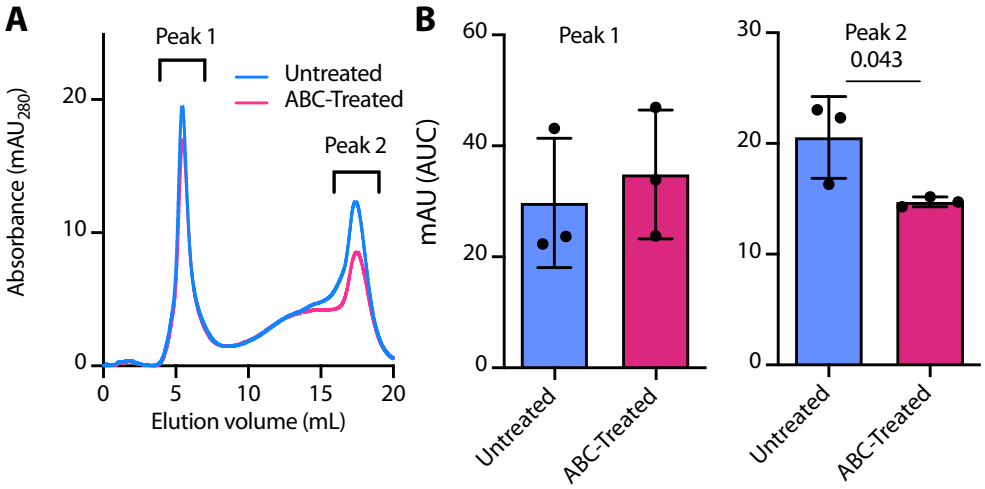

Fig. 4. Anaerobic microbiota alter epithelial mucin integrity. (A) Representative FPLC traces of MUC5AC mucins purified from Calu-3 cells grown under DOAC conditions (untreated) and after treatment with an anaerobic bacterial community. **(B)** Area under curve (AUC) for both peak 1 (high molecular weight mucins) and peak 2 (low molecular weight mucin). Data shown were derived from three independent experiments using three biological replicates (n=9). Data were compared using a unpaired t-test with Welch's correction (**, $p<0.01$).

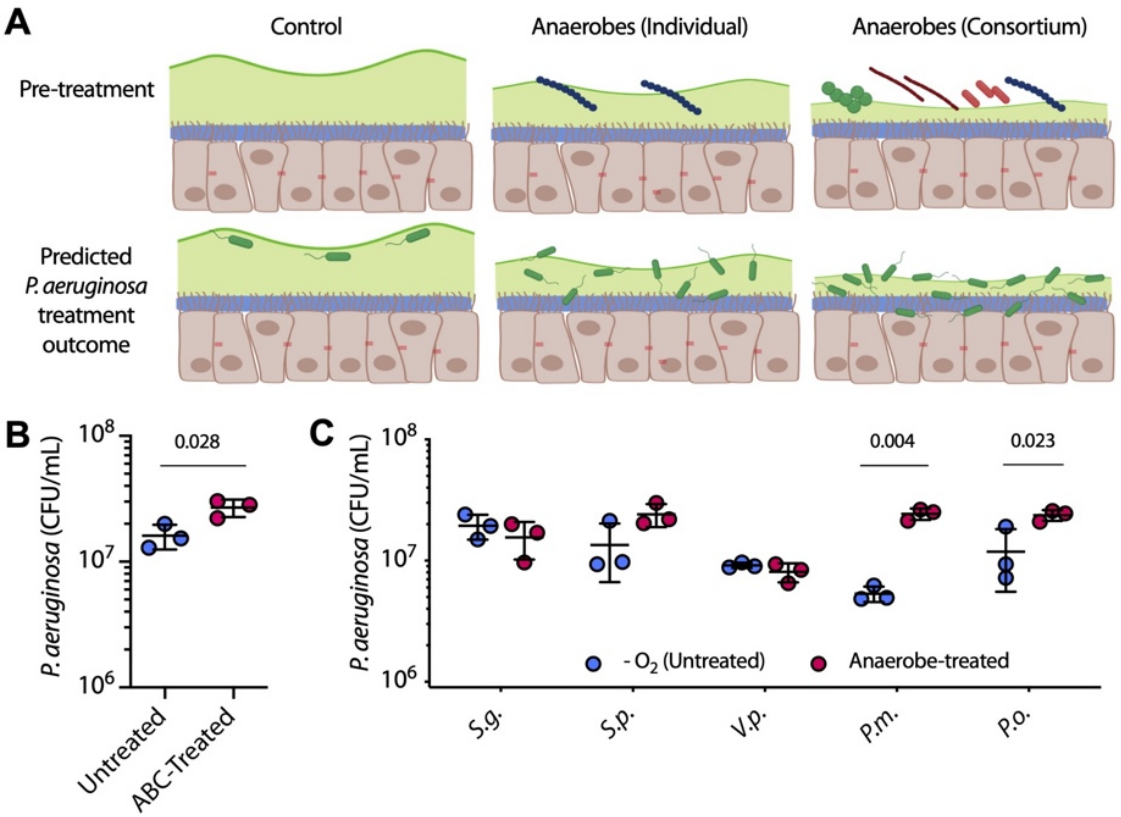

Fig. 5. Anaerobic microbiota condition the epithelial interface for pathogen colonization. (A) Schematic of experimental design and expected outcomes. **(B)** Calu-3 pre-treatment with an anaerobic bacterial consortium (ABC-treated) potentiates *P. aeruginosa* colonization. **(C)** *P. aeruginosa* adhesion to Calu-3 cells after pre-treatment with individual anaerobes (*S.g., Streptococcus gordonii; S.p., S. parasanguinis; V.p., Veillonella parvula; P.o., Prevotella oris; P.m., P. melaninogenica)*. Data shown in panels B and C were derived from three independent experiments with three biological replicates (n=9). Pairwise comparisons in panel D were performed using an unpaired t-test with Welch's correction.

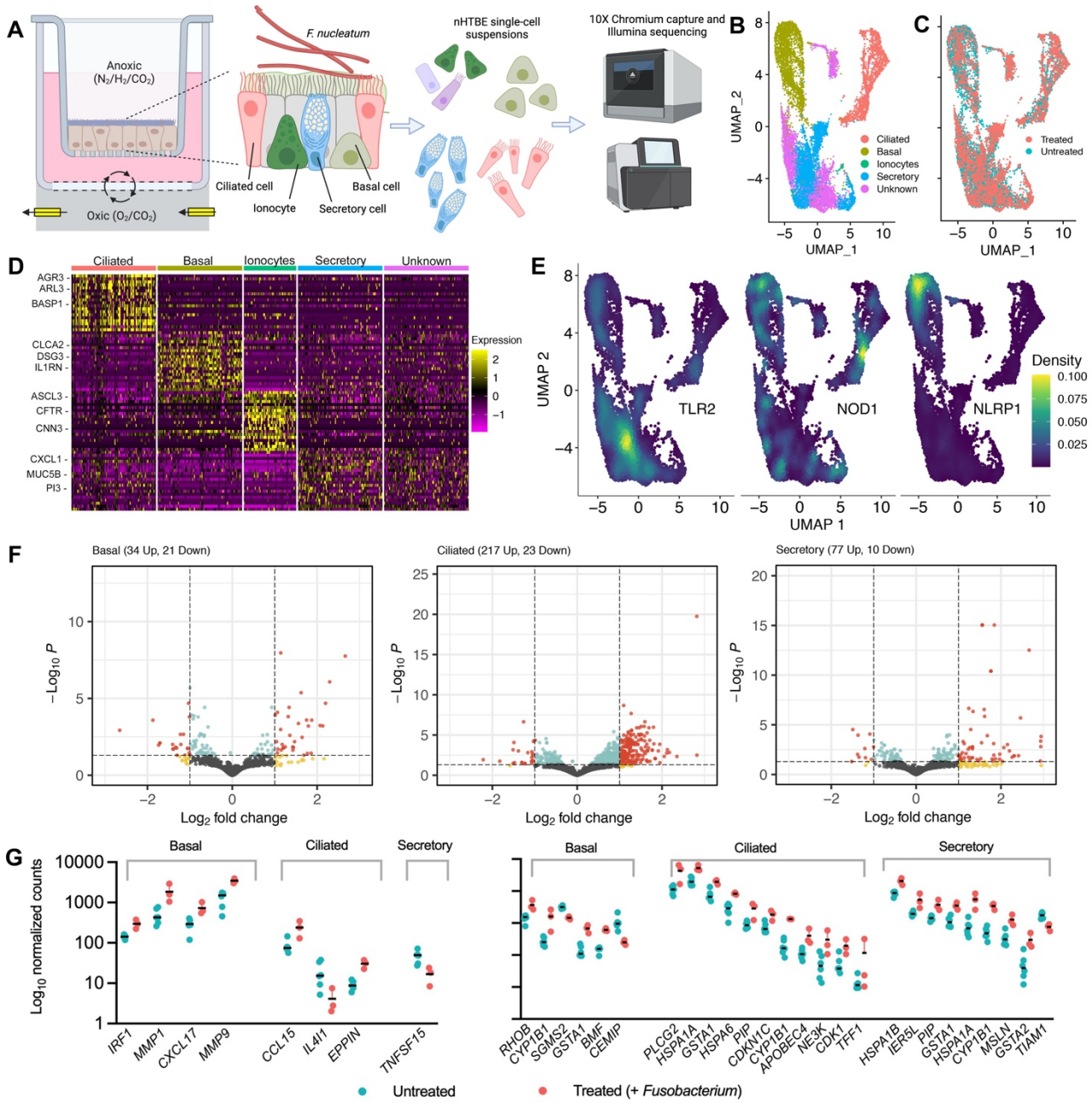

Fig. 6. Single cell RNA sequencing. (A) Experimental schematic. Primary airway epithelial cells were cultured under DOAC conditions and challenged with *F. nucleatum*. Host cells were dissociated and collected via the 10X Genomics platform prior to scRNAseq. (**B**) UMAP projection of nHTBEs showing 4 major cell types (and unknown cells) from 13 distinct clusters (see Fig. S3). **(C)** UMAP projection of nHTBE cell types by treatment condition. **(D)** Scaled expression of the top DEGs that informed specific cell subsets. **(E)** Density plots (Nebulosa projections) of TLR2, NOD1, and NLRP1 showing heterogeneous expression of pattern recognition receptors between cell types. **(F)** Volcano plot representation of differential gene expression in basal, ciliated, and secretory cells between *F. nucleatum*-treated nHTBE cultures relative to untreated controls. **(G,H)** Scatterplot representations of differentially expressed (**G**) inflammatory markers (left panel) and cancer-associated genes (right panel) by cell type.